H_2S Gas Interaction with Pt(II)-Containing Polymetallaynes of Selected Chain Length: An XPS and EXAFS Study

Chiara Battocchio,*,† Ilaria Fratoddi,‡ Maria Vittoria Russo,‡ and Giovanni Polzonetti†

Department of Physics and Unità INSTM and CISDiC, University "Roma Tre", Via della Vasca Navale, 84 - 00146 Rome, Italy, and Department of Chemistry, University of Rome "La Sapienza", P.le A. Moro 5 - 00185 Rome, Italy

Received: April 10, 2008; Revised Manuscript Received: June 3, 2008

The interaction between gaseous H_2S and the surface of several metal-containing oligomers, investigated by emission and absorption spectroscopies, is presented and discussed. The polymetallayne *trans*-{Cl-[Pt(PBu_3)$_2$(C≡C−C_6H_4−C_6H_4−C≡C)]$_9$Pt(PBu_3)$_2$Cl} and related model molecules, i.e. the binuclear transition metal dialkynyl bridged Pt(II) square planar complex *trans*,*trans*-[ClPt(PBu_3)$_2$(C≡C−C_6H_4−C_6H_4−C≡C)-Pt(PBu_3)$_2$Cl], the tetranuclear linear oligomer *trans*-{Cl-[Pt(PBu_3)$_2$(C≡C−C_6H_4−C_6H_4−C≡C)]$_3$Pt(PBu_3)$_2$Cl}, the tetranuclear cyclic oligomer *cis*-[Pt(PBu_3)$_2$(C≡C−C_6H_4−C_6H_4−C≡C)]$_4$, were exposed to hydrogen sulfide and then investigated by X-ray photoelectron (XPS) and X-ray absorption (XAS) spectroscopies, in order to shed light on the gas/polymer interaction associated to the sensing properties of these materials. XPS measurements evidenced the presence of S in the polymetallayne samples exposed to H_2S, and the measured S2p binding energy values correlate with H_2S adsorbed by means of sulfur atoms chemically bonded to metal atoms, owing to the formation of sulfur-containing adducts. XAS data analysis suggested a square-pyramidal geometry around the transition metal with H_2S in the apical position for the pentacoordinated platinum units.

Introduction

Sulfur-containing compounds are common impurities in fossil-derived fuels and chemical feed stocks[1] and damage the quality of the air by forming sulfur oxides SO_x during the burning of fuels, which are major air pollutants leading to acid rain.[2] In addition, the sulfur impurities are responsible for the rapid deactivation or poisoning of most catalysts and for the corrosion of equipment used in the chemical and petrochemical industries.[3] Therefore, the detection and monitoring of sulfur-containing compounds are highly attractive.[4,5] Among others, hydrogen sulfide (H_2S) is a toxic and malodorous gas, contained in oil or natural gas mines, that has been proved very harmful to the human body and to the environment and whose detection and monitoring are of high importance for both resource exploitation and human health. In recent times, a number of semiconductor sensors have been found to be sensitive to H_2S, including SnO_2, WO_3, In_2O_3, ZnO_2, a few perovskite-type materials such as $NdFeO_3$ or $NiFeO_4$, and Pt-doped α-Fe_2O_3 powders.[6] The application of these sensors is however limited by some disadvantages such as the poor selectivity, long response time, and high operating temperature or limited detection range.

Traditionally used semiconducting materials are being replaced with organic and organometallic compounds in specific application as the one presently discussed. The low cost, processability, and versatility of organic and organometallic oligomers and polymers are, among others, the parameters that make these materials convenient and advantageous for replacing the traditional ones.

Organometallic Pt-containing macromolecules such as square-planar Pt(II) complexes tend to coordinate sulfur-containing molecules, giving rise to pentacoordinated adducts; actually, sulfur dioxide is a versatile ligand in organic and inorganic chemistry, as it can be active as both a Lewis base or acid. For example, a series of square-planar Pt(II) complexes has been successfully tested as SO_2 sensors and found highly selective and particularly selective for submillimolar to molar gas quantities.[7] Solid-state crystal structure of the SO_2 adducts showed a square-pyramidal geometry around the metal center with SO_2 in the apical position.[7]

Because of its electronic structure, hydrogen sulfide is expected to interact with Pt centers in square-planar Pt(II) complexes as an electron donor (Lewis base); in addition, a fine-tuning of the electrophilicity of the metal center, by electronic and steric modifications of the ligand array in the pristine complex, would predictably influence the H_2S coordination, thus influencing the reversibility of the linkage and the optical response of the new molecular adduct.

Since the past decade, the electronic, optical, and liquid crystal applications of "rigid-rod" organometallic polymers, obtained from transition-metal complexes with alkynyl ligands, have been thoroughly investigated,[8] and the correlated intrachain electron and hole migration of model Pt alkynyl mixed valence complexes have been elucidated,[9] as well as the charge transport in molecular model Pt acetylides,[10] in view of their applications as components for molecular electronics. The research of our group has been focused on investigations of the chemical and electronic structure of Pt-containing *rod-like* organometallic polymers[11] and also diethynyl organic spacers that are the building blocks of these materials.[12] In this framework, binuclear complexes and small oligomers have been successfully used as model molecules for the interpretation of the optoelectronic properties of more complicated systems.[13] In the field of

* Corresponding author. Telephone: (+) 39-06-55173388, fax: (+) 39-06-55173390, e-mail: battocchio@fis.uniroma3.it.
† University "Roma Tre".
‡ University of Rome "La Sapienza".

10.1021/jp803119j CCC: $40.75
Published on Web 07/23/2008

technological applications, sensor devices based on sensitive membranes made from rigid rod organometallic molecules in the form of self-assembled (SAMs) monolayers can be successfully implemented. For example, Pt polyynes have been used as thin film membranes in surface acoustic wave (SAW) devices[14] showing high sensitivity toward relative humidity and sulfur-containing organic vapors.[15] Recent studies on sensors based on analogue polymetallaynes showed a higher sensitivity toward low relative humidity percentages, when nanostructured membranes were employed.[16] The obtained materials have been extensively studied and conveniently used as sensors; however, the basic understanding of some chemical and physical aspects must still be investigated.

In this paper, we report information achieved about the interaction occurring between H_2S and a series of Pt-containing molecules. The here considered samples are the binuclear transition metal dialkynyl bridged Pt(II) complex *trans*,*trans*-[ClPt(PBu_3)$_2$(C≡C−C_6H_4−C_6H_4−C≡C)Pt(PBu_3)$_2$Cl] (**1**), the tetranuclear linear oligomer *trans*-{Cl-[Pt(PBu_3)$_2$(C≡C−C_6H_4−C_6H_4−C≡C)]$_3$Pt(PBu_3)$_2$Cl} (**2**), the tetranuclear cyclic oligomer *cis*-[Pt(PBu_3)$_2$(C≡C−C_6H_4−C_6H_4−C≡C)]$_4$ (**3**), and the multinuclear (10 Pt-containing units) linear oligomer *trans*-{Cl-[Pt(PBu_3)$_2$-(C≡C−C_6H_4−C_6H_4−C≡C)]$_9$Pt(PBu_3)$_2$Cl} (**4**). These systems were investigated by a combined X-ray photelectron (XPS) and X-ray absorption (XAS) spectroscopy probing the electronic structure of both oligomer and adsorbate molecules as well as the geometric arrangement of the whole system.

On the basis of previously achieved results concerning the specific sensing properties of platinum poly ynes to H_2S,[15] in the framework of an extensive investigation as a starting approach we have considered reaction conditions that guarantee the grafting of H_2S to the Pt-containing systems; however, our planning considers further investigations in more controlled exposure conditions.

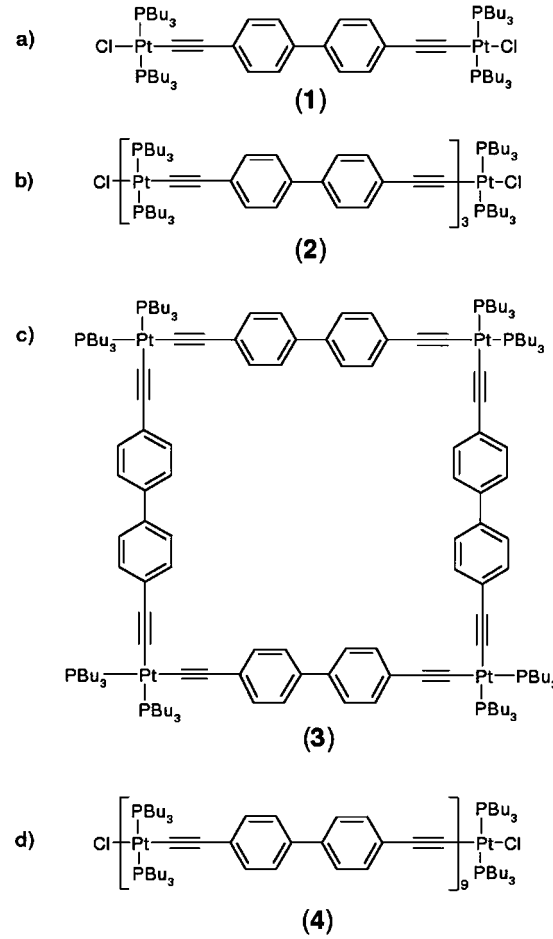

Figure 1. Molecular structures of *trans*,*trans*-[ClPt(PBu_3)$_2$-(C≡C−C_6H_4−C_6H_4−C≡C−Pt(PBu_3)$_2$Cl] (**1**), *trans*-{Cl-[Pt(PBu_3)$_2$-C≡C−C_6H_4−C_6H_4−C≡C]$_3$ Pt(PBu_3)$_2$ Cl} **2**, *cis*-{[Pt(PBu_3)$_2$-C≡C−C_6H_4−C_6H_4−C≡C]$_3$ Pt(PBu_3)$_2$] (**3**), and *trans*-{Cl-[Pt(PBu_3)$_2$C≡C−C_6H_4−C_6H_4−C≡C]$_9$ Pt(PBu_3)$_2$ Cl} (**4**).

Experimental Section

Materials and Methods. Complex **1** and oligomers **2** and **4** were synthesized as reported in previous papers,[17,18] by following a dehydrohalogenation procedure, involving the reaction of *trans*-[Pt(PBu_3)$_2$Cl$_2$] square-planar complexes with the 4,4′-diethynylbiphenyl (DEBP) monomer in the presence of diethylamine as the solvent. Complex **3**, *cis*-{[Pt(PBu_3)$_2$C≡C−C_6H_4−C_6H_4−C≡C]$_4$, was prepared by slightly changing the dehydrohalogenation reaction, and the experimental conditions and main spectroscopic characterizations are reported:

A 0.40 g (0.6 mmol) amount of *cis*-[Pt(PBu_3)$_2$Cl$_2$] and 0.12 g (0.6 mmol) of DEBP were dissolved in 30 mL of diethylamine, CuI was then added (5.0 mg, 0.03 mmol), and the reaction was run at $T = 25$ °C for 3 h. From the reaction mixture, the product **3** was extracted from CH_2Cl_2/H_2O, and the organic phase was dried and then purified by chromatography on SiO_2 with an eluant mixture petroleum ether/THF 5/1. The eluted fraction containing compound **3** was dried and characterized (0.39 g, 0.12 mmol, yield 63%): UV (nm, $CHCl_3$): 340.8; FTIR (cm^{-1}, nujol mulls): 2113 (ν C≡C), 1901, 1602 (ν C=C); ^{1}H NMR (δ ppm, $CDCl_3$): 0.91 (t, CH_3), 1.42 (q, $CH_2CH_2CH_3$), 1.51 (m, $CH_2CH_2CH_3$), 2.01 (m, PCH_2), 7.41 (ArH),7.28 (ArH); ^{31}P NMR (δ ppm, $CDCl_3$): −2.43, (J_{P-Pt} = 2249 Hz); Elemental analyses, found (calculated) for $C_{160}H_{248}P_8Pt_4$ (%): C = 59.42 (60.22), H = 8.01 (7.78). Mass spectrum: 3191 *m*/*z*. (calculated 3188).

Adduct Formation with Hydrogen Sulfide. The exposure of complex **1** and oligomers **2**, **3**, and **4** to 500 mbar of H_2S (Air Liquide, 99.95%) was carried out in a chemical cell equipped with input and output gas lines, that allowed EXAFS measurements to be performed on samples in controlled chemical environment. Samples were finely ground and mixed with cellulose; the powder was then pressed by means of a hydraulic press equipped with a Specap P/N 10 mm evacuable pellet die. The pellets of samples **1**−**4** were successively exposed to H_2S gas, and a characteristic color change, for all of the samples, from white/light yellow to orange/brown was indicative for the gas absorption producing a chemical reaction then leading to the formation of a new molecular species.

Spectroscopic Characterizations. FTIR spectra were recorded as nujol mulls or as films deposited from $CHCl_3$ solutions by using CsI cells, on a Bruker 70 Fourier transform spectrometer. ^{1}H and ^{31}P NMR spectra were recorded in $CDCl_3$ on a Bruker AC 300P spectrometer at 300 and 121 MHz, respectively; the chemical shifts (ppm) were referenced to TMS for ^{1}H NMR assigning the residual ^{1}H impurity signal in the solvent at 7.24 ppm ($CDCl_3$). ^{31}P NMR chemical shifts are relative to H_3PO_4 (85%). Elemental analyses were performed at the Department of Chemistry, University of Rome "La Sapienza.

UV−vis spectra were recorded on a Cary 100 Varian instrument. All measurements were performed at room temperature using quantitative $CHCl_3$ solutions of the samples before and after H_2S exposition.

X-ray Photoelectron Spectroscopy. XPS analysis was performed in an instrument of our own design and construction, consisting of a preparation and an analysis chamber, equipped

	$Pt4f_{7/2}$ (Pristine Sample)		$Pt4f_{7/2}b$ (Sample + H_2S)	
	B.E. (eV)	FWHM (eV)	B.E. (eV)	FWHM (eV)
(1)	73.00	1.90	73.10	1.96
(2)	73.10	2.00	73.13	1.92
(3)	73.10	2.03	73.09	1.95
(4)	73.13	1.90	73.13	1.92

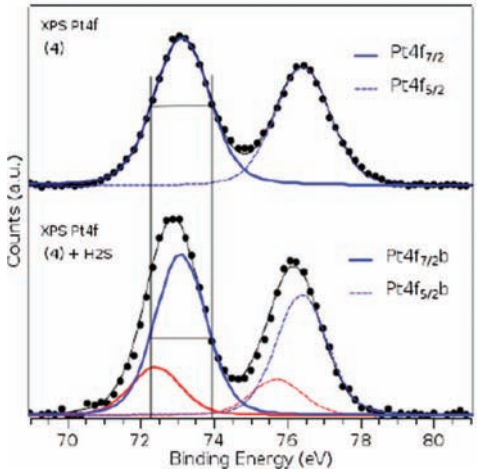

Figure 2. Pt4f XPS spectra collected on sample **4** prior and after exposure to H_2S gas. For all the treated samples, the overall signal is wider, and a small asymmetry, arising by the new spectral component, is detectable at lower BE. It is noteworthy that the component ascribed to the pristine Pt poly yne ($Pt4f_{7/2}b$, higher BE values) in the spectrum collected on the treated sample shows the same BE and fwhm values of the pristine sample spectrum. BE and fwhm values for Pt4f signals of all samples, both pristine and interacting with H_2S (*b* component), are reported in the included table.

with a 150 mm mean radius hemispherical electron analyzer with a four-elements lens system with a 16-channel detector giving a total instrumental resolution of 1.0 eV as measured at the Ag $3d_{5/2}$ core level. Mg Kα nonmonochromatized X-ray radiation ($h\nu$ = 1253.6 eV) was used for acquiring core level spectra of both substrate and adsorbate samples (C1s, P2p, Pt4f, Cl2p, and S2p). The spectra were energy referenced to the C1s signal of aromatic C atoms having a binding energy BE = 285.00 eV. Atomic ratios were calculated from peak intensities by using Scofield's cross-section values and calculated λ factors.[19] Curve-fitting analysis of the C1s, P2p, Pt4f, S2p, and Cl2p spectra was performed using Voigt profiles as fitting functions, after subtraction of a Shirley-type background.[19,20] XPS measurements were carried out on complex **1** and oligomers **2**, **3**, and **4** before and after gas exposure. Measurements on the pristine samples were performed on thin films, obtained by spin-depositing onto Si(111) wafers surfaces at 700 rpm for 10 s dichloromethane solutions of **1**−**4**. H_2S exposure was performed, as described in section 2.1, on solid samples mixed with cellulose and a first series of XPS data was collected on these pellets. As a purpose of comparison, X-ray photoelectron spectroscopy was also performed on thin films obtained by spinning dichloromethane solutions of samples **1**−**4**, after H_2S exposure, on Au/Si(111) substrates. CH_2Cl_2 solutions of samples **1**, **2**, **3**, and **4** after H_2S exposure were obtained by percolating the solvent through the cellulose-containing pellets. Since the cellulose is not dissolved by dichloromethane, the solutions obtained following this procedure contain the organometallic samples only. XPS data collected on pellets and films (i.e., with and without cellulose) gave identical S2p, P2p, Pt4f, Cl2p core level spectra.

Extended X-ray Absorption Fine Structure (EXAFS). EXAFS[21] experiments were performed at ESRF storage ring at the GILDA CRG beamline. The monochromator was equipped with two Si(311) crystals,[22] and harmonic rejection was achieved by using a pair of Pd-coated mirrors with a cutoff energy of 20.2 keV. Data were collected in transmission mode. For the X-ray absorption spectroscopy (XAS) measurements, pellet samples of the macromolecules mixed with cellulose were prepared.

EXAFS measurements were initially performed in low vacuum conditions ($P = 10^{-3}$ mbar) on the pristine samples. Removal of contaminants in the chemical cell system was achieved by several cycles of pumping and filling with H_2S; a final filling with hydrogen sulfide was then made up to a partial pressure of about 500 mbar, and EXAFS structural characterization was carried out again. *In situ* treatments could be performed at the GILDA beamline by means of a small chemical cell equipped with a gas line, built on purpose.[23] In the framework of our study, as a first step the choice of high gas pressure in the chemical cell (500 mbar) was made in order to guarantee that a chemical interaction arises between the organometallic molecule and H_2S gas, leading to the formation of an adduct whose molecular structure study is the main topic of this research work at this stage. EXAFS measurements in H_2S environment started as soon as the cell was filled up with gas, and at least four EXAFS spectra were collected on each sample. A good resolution EXAFS spectrum at the Pt-L_{III}-edge require nearly 45 min to be collected; therefore, we can estimate that each sample was exposed to H_2S for about 2 h. However, a comparison between spectra recorded in sequence on the same sample showed that these were identical to each other; this result was indicative for an interaction between Pt-containing materials and hydrogen sulfide relatively fast that gives rise to a chemical species quite stable in the reported experimental conditions.

XAS data in the so-called *extended* region were extracted with the AUTOBK code[24] by linear fitting of the pre-edge region and subtraction of the atomic background fitted with a cubic *spline*. Theoretical XAS signals were generated using ARTEMIS[25] software with FEFF8.20[26] calculations, starting from the cluster obtained by X-ray diffraction measurements of the *trans*-$[ClPt(PBu_3)_2(C{\equiv}C{-}C_6H_4{-}C_6H_4{-}C{\equiv}C{-}Pt(PBu_3)_2Cl]$ sample.

Results and Discussion

Pristine Materials Characterization. The dinuclear complex *trans*,*trans*-$[ClPt(PBu_3)_2(C{\equiv}C{-}C_6H_4{-}C_6H_4{-}C{\equiv}C)Pt(PBu_3)_2Cl]$ (**1**), the tetranuclear linear oligomer *trans*-$\{Cl[Pt(PBu_3)_2(C{\equiv}C{-}C_6H_4{-}C_6H_4{-}C{\equiv}C)]_3Pt(PBu_3)_2Cl\}$ (**2**), the tetranuclear cyclic oligomer *cis*-$[Pt(PBu_3)_2(C{\equiv}C{-}C_6H_4{-}C_6H_4{-}C{\equiv}C)]_4$ (**3**), and the multinuclear (10 Pt units) linear oligomer *trans*-$\{Cl[Pt(PBu_3)_2(C{\equiv}C{-}C_6H_4{-}C_6H_4{-}C{\equiv}C)]_9Pt(PBu_3)_2Cl\}$ (**4**), whose molecular structures are reported in Figure 1, were fully characterized by means of XPS, EXAFS, and UV−visible absorption spectroscopies before exposure to H_2S. Among them, the novel compound **3** was isolated and fully characterized. The formation of a cyclic structure was achieved in analogy with analogous Pt(II) complexes[27] and confirmed by means of mass spectrometry and NMR spectroscopy. In particular, in the ^{31}P NMR spectrum, a signal at −2.43 ppm was found, with a coupling constant J_{P-Pt} equal to 2249 Hz, typical of cis square-planar complexes.[28]

TABLE 1: EXAFS Data Analysis Results for Pristine Samples 1−4[a]

scattering path		1	2	3	4
single scattering Pt−C_1	R	1.96(2)	1.99(5)	1.96(2)	2.00(8)
	$\sigma \times 10^4$	45(5)	81 (6)	45(5)	29(4)
single scattering Pt−P	R_1	2.31(3)	2.29(7)	2.31(3)	2.31(2)
	$\sigma_1 \times 10^4$	30(4)	81(6)	30(4)	27(2)
single scattering Pt−C_2, double scattering Pt−C_2−C_1, triple scattering Pt−C_1−C_2−C_1	R_2	3.16(8)	3.19(4)	3.16(8)	3.21(4)
	$\sigma_2 \times 10^4$	72(2)	113(1)	72(2)	48(4)
single scattering Pt−Cl	R_3	2.26(4)	1.97(9)	2.26(4)	-
	$\sigma_3 \times 10^4$	826(5)	84(6)	826(5)	-
R-factor		0.010	0.018	0.020	0.020

[a] R is in angstroms, σ is in 10^{-4} Å^2. The numbers in parentheses are the uncertainties in the interatomic distances and DW factors. EXAFS data for **1** and **4** (ref 18) are also reported for comparison. For each sample, the global amplitude factor $S0^2$ and the edge position ΔE_0 were fixed to the best-fit values and are the same for all the considered paths. R-factor is a least-squared residual, showing the goodness of fit.

X-ray photoelectron spectroscopy and UV−visible absorption measurements of samples **1**, **2**, and **4** have been already performed and discussed by some of us,[17] giving evidence of the electronic delocalization through the transition metal 6p and 5d orbitals, that was expected on the basis of theoretical studies on the band structure of organometallic polymetallaynes.[29]

Recently, XPS measurements of C1s, Pt4f, and P2p core levels have been also performed on the newly synthesized sample **3**, and the observed spectra are completely similar to those acquired on samples **1**, **2**, and **4** and discussed in reference 17 as expected. In fact, the $Pt4f_{7/2}$ spin orbit component peak of sample **3** occurs at 73.10 eV binding energy (BE), with a full width at half maximum (fwhm) of 2.03 eV and is therefore fully consistent with $Pt4f_{7/2}$ components already observed for **1**, **2**, and **4** (see Figure 2 and included table). The evaluation of atomic ratios by means of XPS confirmed the calculated stoichiometry and allowed to assess the number of repetitive units of all samples; furthermore, measurements performed after aging the samples for several months lead to establish the environmental stability of these Pt-containing materials.[17]

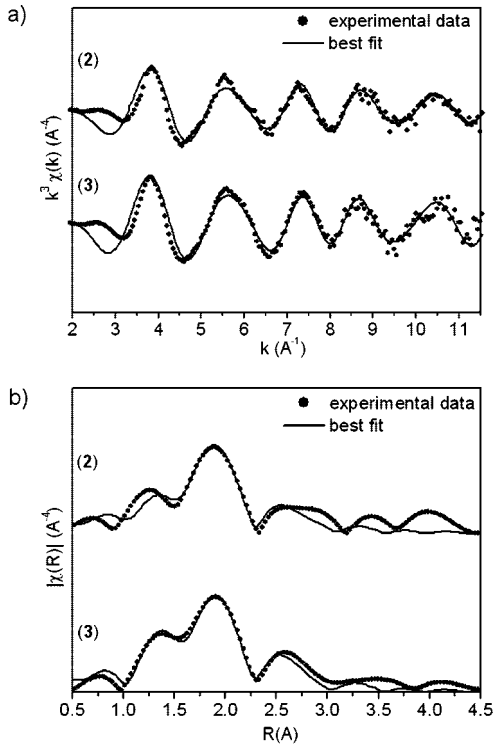

Figure 3. (a) EXAFS signal weighted with k^3 for **2** and **3** and respective best fits; (b) Fourier transformation of the EXAFS signal in R space and best fits for **2** and **3**.

In addition, a joint X-ray diffraction and EXAFS study was carried out on complex **1**,[18] leading to assessment of the square-planar geometry of the metallic center. The XRD diffraction parameters obtained for sample **1** were also used at that time as a basis set for the elaboration of EXAFS data collected on the ten units oligomer **4**, i.e. *trans*-{Cl-[Pt(PBu_3)$_2$-C≡C−C_6H_4−C_6H_4−C≡C]$_9$Pt(PBu_3)$_2$Cl}, whose crystal structure could not be obtained because of its amorphous nature, and allowed us to establish the square-planar geometrical arrangement of the acetylene moieties and of the tributyl phosphine groups around the transition metal. Referring to this model, the Pt atom is four-coordinated with two P atoms (which in the full molecule are tributylphosphine units) and two acetylene units (that belong to the diethynyl-biphenyl moieties DEBP).

In the present work, the method of data analysis previously developed[18] has been fruitfully applied in order to investigate the molecular structure of samples **2** and **3**. In order to analyze the EXAFS data collected on samples **2** and **3** at the Pt-L_{III}-edge, i.e. in the 11400−12600 eV energy region, contribution to the total signal from the P_1, P_2, C_1, C_2, C_{11}, and C_{21} atoms have been considered by including the single (Pt−C_1, Pt−C_2, Pt−C_3, Pt−P_1), double (Pt−C_1−C_2) and triple (Pt−C_1−C_2−C_1) linear scattering paths for the photoelectron. In order to describe the single scattering (SS) involving the Pt, C_1, P, C_2, and Cl atoms, i.e. Pt−C_1, Pt−P, and Pt−C_2, respectively, the bond length and Debye−Waller (DW) factors R, σ, R_1, σ_1, R_2, σ_2, R_3, σ_3 were used; each path has a 2-fold degeneration, reflecting the presence of two P and two acetylene groups around Pt. The multiple scattering (MS) paths Pt−C_2−C_1−Pt and Pt−C_1−C_2−C_1−Pt were also considered with parameters R_2, σ_2. This is justified by the fact that the atomic configuration Pt−C_1−C_2 is collinear so the path of the SS and MS paths are strictly the same. The use of a common DW factor is an approximation that permits a limited number of free parameters. Fits of the data have been carried out in R space after Fourier transform of the k weighted EXAFS data in the range $k = 3.0-11.5$ Å^{-1}, while the R range for the fits was R=1.1−4.0 Å. $S0^2$ and ΔE_0 have been fixed to the best-fit values, and the resulting values for the atomic distances R, R_2, R_3 and relative Debye−Waller factors σ, σ_2, σ_3 are listed in Table 1. The overall quality and suitability of the fits was also evaluated by ARTEMIS[25] software and is shown as the "R-factors" in Table 1. In the present case R factors in the range 0.010−0.020 have been obtained, thus evidencing the goodness of the analysis; as a rule it is generally

TABLE 2: XPS Data Collected on Samples 1−4 after Exposure to H_2S Gas

	pellet[a]			$CHCl_3$ solution			
	BE (eV)	fwhm (eV)	A/σ	BE (eV)	fwhm (eV)	A/σ	average atomic ratios
Complex **1**							
C1s	285.00			285.00	1.87	4713	C/Pt(tot) = 38.2
$P2p_{3/2}$	131.23	1.88	264.5	131.23	1.86	301.9	P/Pt(tot) = 2.2
$Pt4f_{7/2}$	72.43	1.96	42.8	72.34	1.94	44.0	Pt(a) = 35%
	73.22	1.96	78.9	73.10	1.94	79.5	Pt(b) = 65%
$S2p_{3/2}$	162.26	2.14	45.1	162.29	2.07	42.8	Pt(a)/S ≈ 1.0
$Cl2p_{3/2}$	198.45	1.74	97.9	198.47	1.68	101.4	Cl/Pt(tot) = 0.8
Oligomer **2**							
C1s	285.00			285.00	1.91	5037	C/Pt(tot) = 51.4
$P2p_{3/2}$	131.23	1.90	169	131.23	2.03	251	P/Pt(tot) = 2.4
$Pt4f_{7/2}$	72.28	1.92	32.4	72.33	1.89	34.0	Pt(a) = 33%
	73.09	1.92	59.3	73.13	1.89	67.9	Pt(b) = 67%
$S2p_{3/2}$	162.23	1.79	29.9	162.03	2.06	35.4	Pt(a)/S = 1.0
$Cl2p_{3/2}$	198.13	2.02	47.0	198.56	1.82	64.0	Cl/Pt(tot) = 0.5
Oligomer **3**							
C1s	285.00			285.00	1.70	3917	C/Pt(tot) = 50.5
$P2p_{3/2}$	131.21	2.06	120	131.21	1.99	164	P/Pt(tot) = 2.2
$Pt4f_{7/2}$	72.45	1.95	17.9	72.38	1.92	25.1	Pt(a) = 34%
	73.25	1.95	32.8	73.09	1.92	52.5	Pt(b) = 66%
$S2p_{3/2}$	162.15	2.14	18.0	162.32	2.48	27.8	Pt(a)/S ≈ 1.0
Oligomer **4**							
C1s	285.00			285.00	1.87	3322	C/Pt(tot) = 41.4
$P2p_{3/2}$	131.28	1.88	155	131.28	1.98	163.2	P/Pt(tot) = 2.0
$Pt4f_{7/2}$	72.41	1.92	30.8	72.42	1.93	27.5	Pt(a) = 34%
	73.26	1.92	60.0	73.13	1.93	52.7	Pt(b) = 66%
$S2p_{3/2}$	162.38	2.63	27.0	162.29	2.25	31.7	Pt(a)/S = 1.0

[a] The main component of XPS C1s spectra collected on pellets is the cellulose signal.

accepted that the fit is reliable for *R* factor values lower than 0.050.[30] EXAFS spectra in *K* space ($\chi(k) \times$ K3) and the related Fourier transforms ($\chi(R)$) are reported together with the relative best fits in Figure 3a and Figure 3b, respectively

Best fit results that are collected in Table 1 show a very slight difference between atomic distances and DW factors already found for complex **1** and oligomer **4** and the same parameters estimated for samples **2** and **3**, confirming that the square-planar geometrical arrangement of the acetylene moieties and of the tributyl phosphine groups around the transition metal already assessed for the model molecule **1** and oligomer **4**[18] are preserved in both tetranuclear samples.

Samples Characterization during and after Interaction with H_2S. Complex **1** and oligomers **2**, **3**, and **4** were exposed to H_2S gas as reported in the Experimental Section. EXAFS, XPS, and UV−visible absorption measurements have been performed on all the samples after gas treatment, and the comparison between the obtained spectra and those measured for the pristine materials lead to ascertain that are the Pt centers undergoing chemical perturbation being involved in the interaction of Pt poly ynes with H_2S.

XPS. XPS measurements of C1s, P2p, Cl2p, S2p, and Pt4f core levels were carried out after H_2S exposure on both cellulose pellets and thin films (obtained by spinning CH_2Cl_2 solutions on Au/Si(111) substrates) for all the four samples considered here; the two series of experiments (cellulose pellet and thin film) gave the same results, indicating that cellulose does not play any role during the polymer interaction with H_2S. XPS data (BE, fwhm, atomic ratios) collected on complex **1** and oligomers **2**, **3**, and **4** either as pellets or as solutions are reported in Table 2.

Analysis of the Pt4f and S2p signals shed some light on the chemical interaction arising between square-planar Pt(II) centers and H_2S molecules, that, as will be shown in the following, is responsible for the well-known sensitivity of Pt poly ynes toward sulfur-containing molecules.[14–16] Pt4f XPS spectra as collected on **1**−**4** pellet samples after exposure to H_2S, are displayed in Figure 4.

XPS Pt4f spectra show a broadening and an asymmetry at lower binding energy that, on the basis of a simple charge potential model which neglects changes in final-state, has been attributed to a component associated with Pt centers showing an increase in the electron density. Considering the data analysis of the Pt4f spectrum, the final state effects could be also responsible of the spectral broadening after interaction, but these might be accounted for only by appropriate calculations. However, as will be shown in the following discussion about XPS data analysis, the conclusion that Pt(II), after linkage to sulfur-containing compounds, undergoes chemical shift toward lower binding energy is supported by literature reports for platinum complexes with ligands bound to the metal through Pt−S bonds.[31–34]

The Pt4f spectral broadening induced to suppose the presence of chemically different Pt sites. By means of a curve-fitting analysis, each Pt4f spin−orbit component of the experimental spectrum of samples **1**−**4** results from the combination of two peaks as associated to two Pt atoms involved in different chemical environments; the first $Pt4f_{7/2}$ component is found at nearly 72.3 eV for all samples, the second one at about 73.0 eV. The signal at higher BE occurs at the same energy value as the $Pt4f_{7/2}$ spin−orbit components observed in the pristine samples, i.e. prior to H_2S exposure. Curve fitting of Pt4f spectra was performed by using four peaks generated by the two spin−orbit components $4f_{7/2}$ and $4f_{5/2}$, separated by a spin orbit coupling constant Δ = 3.3 eV (as reported for the pristine samples [17]) and with the expected area ratios $4f_{7/2}$:$4f_{5/2}$ = 4:3.

By comparing the Pt4f spectra as measured on pristine samples and on samples exposed to H_2S vapors (Figure 2), it is

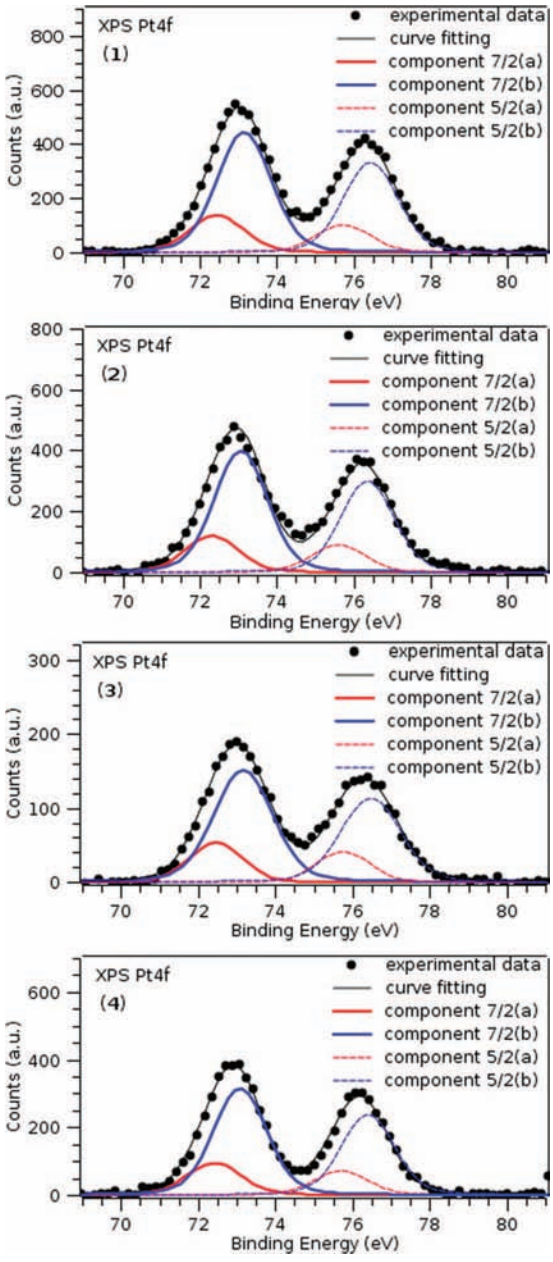

Figure 4. Pt4f XPS spectra collected on samples **1**−**4** after exposure to H_2S gas.

noteworthy that for treated samples the signals become broadened and that they show the presence of a small asymmetry, arising by the new spectral component, at lower BE. Furthermore, for the higher energy Pt4f component both BE and fwhm values, as taken from the Voigt profiles used for peak fitting, are effectively completely similar to the ones observed for pristine samples, as evidenced in Figure 2 for sample **4** and summarized for all samples in the inserted table. On the basis of the above-reported discussion, we assign this Pt signal to the oligomer centers not involved in the reaction taking place with H_2S, then remaining unperturbed.

Conversely, the $Pt4f_{7/2}$ spectral component that occurs at a lower BE value (~72.3 eV) can be associated with Pt metal sites coordinating electron donor ligands, as for instance H_2S; this interpretation appears reasonable and is also in accord with literature data.[31,32] Among others, D. Atzei and co-workers reported a $Pt4f_{7/2}$ BE value of 72.5 eV for the $PtBr_2ttz_2$, $PtCl_2ttz_2$, and $[Pt_3(ttz)_8]C_{16}$ coordination compounds (ttz = 1,3-thiazoli-

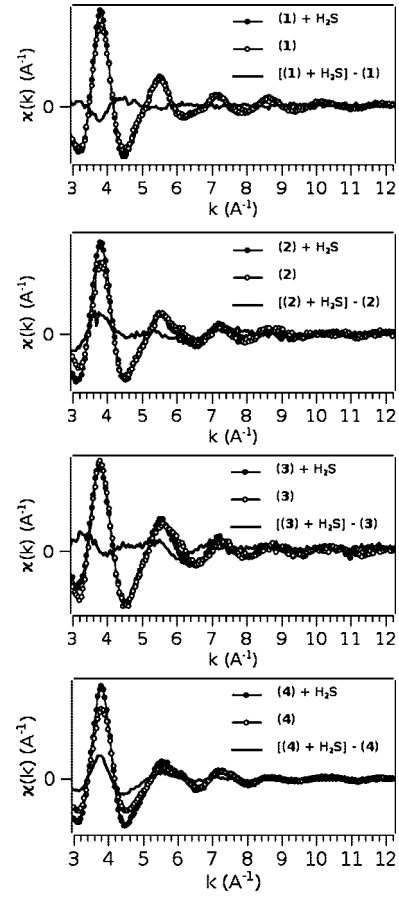

Figure 5. Difference of EXAFS signal in *K*-space before and after H_2S exposure for **1**−**4**. The residue oscillation is attributed to Pt−S bond formation.

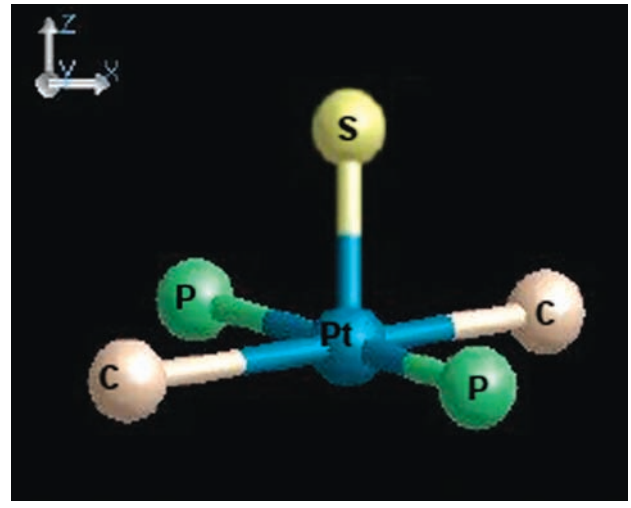

Figure 6. Tridimensional structure of the pentacoordinated Pt(II) cluster. The sulfur atom is in the apical position, on the *z* axis; the two P atoms and the two acetylene units are in the *xy* plane.

dine-2-thione), that was assigned to Pt(II) centers bonded to sulfur.[33,34] Conversely, the $Pt4f_{7/2}$ BE value of the reaction precursor K_2PtCl_4 was 73.0 eV. Thus, an energy shift of nearly 0.5 eV to lower BE values was observed for Pt(II) centers subsequent to Pt−S binding; this finding is in excellent agreement with our Pt4f data.

Support to the above discussion and assignment comes from the analysis of the data relative to the H_2S. We have in fact the evidence that the S2p signal, as measured for all the samples,

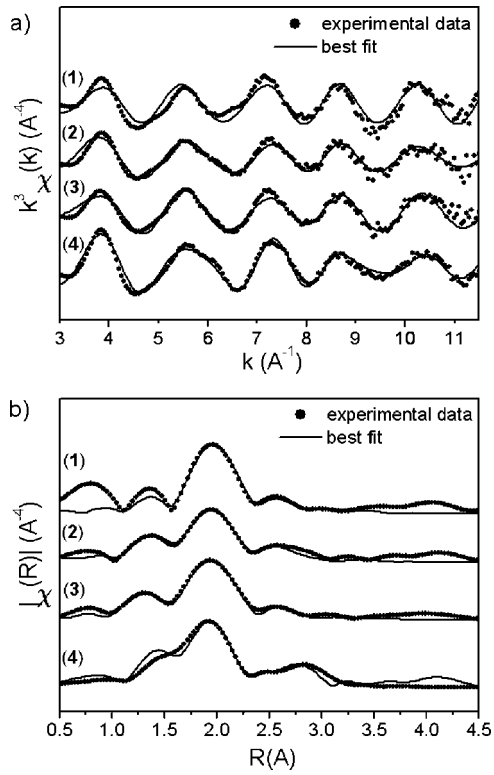

Figure 7. (a) EXAFS signal weighted with k^3 for **1**−**4** and respective best fits; EXAFS data have been collected on samples during exposure to H_2S. (b) Fourier transformation of the EXAFS signal in R space and best fits for **1**−**4** exposed to H_2S.

subsequent to H_2S exposure, occurs at nearly 162.2 eV, a BE value that is significantly different from the one expected for the unperturbed or physisorbed H_2S and that we associate to H_2S chemically interacting with platinum. Our data appear fully consistent with those reported in literature for sulfur-containing molecules interacting with metals through the formation of a sulfur−metal chemical bond[35] as well as for H_2S molecules chemisorbed on metals,[5,36] therefore supporting our assignment. S2p BE for H_2S physisorbed on metals is expected to occur around 164 eV,[5,37,38] a signal which is completely absent in our samples, neither in pellets or thin films.

On the basis of the so far discussed experimental data, we hypothesized that a chemical interaction occurs between samples **1**−**4** and H_2S molecules, involving the formation of a coordination bond between Pt and S. Additionally, as reported in the last column of Table 2, the atomic ratio evaluated between the $Pt4f_{7/2}$ peak at lower BE (72.3 eV) and the S2p signals was estimated as being 1:1 for all samples; this result strongly supports our interpretation because it is in perfect agreement with that expected for the above hypothesized S−Pt bond formation.

Semiquantitative XPS analysis (see Table 2) leads to estimation of the stoichiometry among platinum and adsorbed H_2S. Analysis of the data reported in the last column of Table 2 for all samples shows that the low energy $Pt4f_{7/2}$ component is nearly 33% of the whole $Pt4f_{7/2}$ intensity. This experimental result indicates that under the chosen experimental conditions for gas exposure (H_2S pressure of about 500 mbar in the chemical cell containing the sample pellet) both complex **1** and oligomers **2**, **3**, and **4** exhibit the tendency to react with the same amount of H_2S.

As a hypothesis for why only 1/3 of all Pt centers, as detected by XPS, interact with H_2S, we could say that this is not a case of a single-crystal Pt surface; therefore, we think that the molecular organization at the surface is probably responsible for the partial Pt site involvement in the reaction. Not all the Pt sites are suitably organized at the surface and therefore available for the reaction; nevertheless, excluding an extended H_2S diffusion, all of the Pt sites within a depth of about 60 Å can be detected by the XPS. We have evidence that, under the reported experimental conditions, H_2S−molecule interaction undergoes saturation, meaning that all the Pt sites available for the reaction have been involved. The Pt−H_2S/Pt = 1/3 ratio is then most likely due to steric arrangement of the Pt poly yne molecules.

EXAFS. Extended X-ray absorption fine structure measurements were carried out at the Pt-L_{III}-edge on pellet samples before and during exposure to H_2S. The chemical cell in the measurement chamber was filled with H_2S up to a final pressure of 500 mbar, and considering that the cell volume is about 340 cm^3, an estimate of the gas concentration gives nearly 0.007 mol in the cell and therefore [H_2S] = 20 mmol. The interaction taking place between Pt poly ynes and H_2S, already demonstrated by XPS data analysis, was successively confirmed by the EXAFS results by means of comparison between data collected on the pristine samples and measurements performed in the same energy range on H_2S-exposed samples. Difference EXAFS signals, obtained by subtracting the signal in k space achieved for the pristine poly ynes to the k signal of the corresponding sample as exposed to H_2S, are reported in Figure 5 for samples **1**, **2**, **3**, and, respectively, **4**. The residual oscillation pattern can be reasonably associated with the new Pt−S bond formation and the subsequent reorganization of other bonds.

The theoretical model chosen for fitting the experimental EXAFS data was selected with the aim to take into account the fraction of Pt centers bonded to H_2S, as already estimated by a semiquantitative XPS analysis in 1/3 of the total Pt sites.

As a consequence, for each examined compound the overall Pt-L_{III}-edge EXAFS signal was ascribed as derived by 2/3 (nearly 66%) of square-planar Pt centers (the model used in EXAFS data analysis of pristine samples) and 1/3 (33% approximately) of pentacoordinated pyramidal Pt centers. The pyramidal model was tentatively accounted for by adding a fifth coordination position to the Pt square-planar model; the theoretical Pt−S bond length was hypothesized as 2.53(1) Å, as suggested by XRD measurements performed on similar compounds and previously reported in the literature.[7] A 3D scheme of the square-pyramidal Pt(II) cluster, with the sulfur atom in the apical position and the phosphine groups and acetylene units lying in the xy plane, is shown in Figure 6.

The EXAFS signals $\chi(k)$ weighted for k^3 for samples **1**−**4** as exposed to H_2S molecules are shown in Figure 7a, whereas the associated Fourier transforms are reported in Figure 7b, together with the related best fits. The contribution to the total XAS signal arising from the 66% tetracoordinated Pt centers plus the 33% pentacoodinated transition metal from the atoms C_1, P, C_2, Cl (in samples **1** and **2**) and (for pentanuclear theoretical model P only) S atoms was accounted for by including either the single, double, or triple scattering paths of the photoelectron. In order to describe the single scattering for Pt−C_1, Pt−P, Pt−C_2, Pt−Cl (in samples **1** and **2**) of the tetranuclear theoretical model (T), both bond length and DW factors R_T, σ_T, R_{T1}, σ_{T1}, R_{T2}, σ_{T2}, R_{T3}, σ_{T3} were used. Conversely, in order to describe the single scattering Pt−C_1, Pt−P, Pt−C_2, Pt−Cl (in samples **1** and **2**), and respectively Pt−S of the pentacoordinated (P) model, we employed the bond length and DW factors R_P, σ_P, R_{P1}, σ_{P1}, R_{P2}, σ_{P2}, R_{P3}, σ_{P3}, R_{P4}, σ_{P4}. The multiple scattering paths

TABLE 3: EXAFS Data for 1−4 Exposed to H_2S

scattering path	[a]	1	2	3	4
single scattering Pt−C_1	R_T	1.98(1)	1.92(2)	1.89(8)	2.00(8)
	R_P	1.99(1)	1.96(1)	1.99(8)	2.06(3)
	$\sigma \times 10^4$	14(2)	54(5)	51(4)	79(5)
single scattering Pt−P	R_{1T}	2.33(8)	2.31(2)	2.24(1)	2.31(2)
	R_{1P}	2.34(9)	2.32(4)	2.35(8)	2.37(5)
	$\sigma_1 \times 10^4$	21(7)	49(1)	46(2)	55(2)
single scattering Pt−C_2, double scattering Pt−C_2−C_1, triple scattering Pt−C_1−C_2−C_1	R_{2T}	3.20(1)	3.11(7)	3.06(8)	3.21(4)
	R_{2P}	3.21(7)	3.16(1)	3.23(1)	3.30(2)
	$\sigma_2 \times 10^4$	52(9)	111(3)	197(1)	59(7)
single scattering Pt−Cl	R_{3T}	2.28(7)	2.26(2)	-	-
	R_{3P}	2.29(9)	2.28(5)	-	-
	$\sigma_3 \times 10^4$	21(7)	49(1)	-	-
single scattering Pt−S	R_4	2.58(9)	2.65(3)	2.59(9)	2.61(8)
	$\sigma_4 \times 10^4$	43(1)	113(2)	486(7)	39(6)
R-factor		0.018	0.020	0.020	0.014

[a] R is in angstoms; σ is in 10^{-4} Å^2. The numbers in parentheses are the uncertainties in the interatomic distances and DW factors. For each sample, the global amplitude factor S02 and the edge position ΔE_0 were fixed to the best-fit values and are the same for all the considered paths. The *R*-factor is a least-squared residual, showing the goodness of fit.

TABLE 4: Wavelengths of Maximum Absorption and FWHM of the UV−Visible Spectra Collected on 1−4 before and after Exposure to H_2S Gas

	1	2	3	4
λ_{max} (nm) pristine sample	347.60	360.80	340.80	370.40
λ_{max} (nm) sample + H_2S	347.60	360.80	341.00	370.40
fwhm (nm) pristine sample	53.20	46.15	61.63	43.56
fwhm (nm) sample + H_2S	56.00	50.13	79.62	47.64

Pt−C_2−C_1−Pt and Pt−C_1−C_2−C_1−Pt were also considered by means of the parameters R_{T2}, σ_{T2} and R_{P2}, σ_{P2}, respectively. The overall amplitude was defined as a sum of the two T and P amplitudes, and the ratio AmpT/AmpP = 2/1 was verified to give the best fit results, as suggested by XPS data analysis. Fits of the EXAFS data were carried out in *R* space after Fourier Transform of the k^3 weighted EXAFS data in the range k = 3.5− 11.0 Å^{-1}; the *R* range for all the fits was R = 1.0−3.5 Å, and the bond length (R) and DW factors estimated from best fit using ARTEMIS[25] software with FEFF8.20[26] calculations are reported in Table 3, together with the evaluated *R* factors.

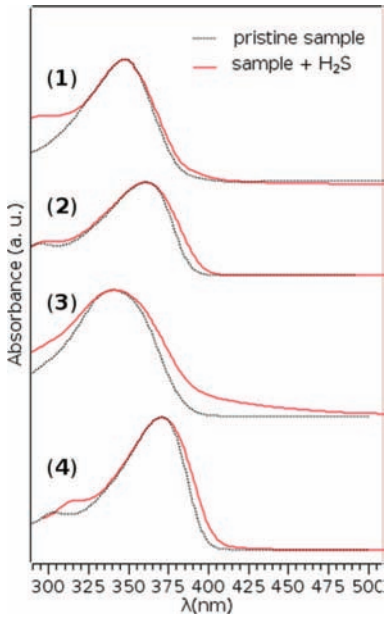

Figure 8. UV−visible spectra collected on **1**−**4** before and after exposure to H_2S gas; in H_2S-containing samples, a fwhm increase due to the interaction between Pt−poly ynes and the hydrogen sulfide molecule is observed.

The hypothesis of the structure reported in Figure 6 can be reasonably justified by coordination chemistry; however, strong support comes from the attempts to fit the EXAFS data of the H_2S-treated samples without sulfur, i.e. with a square planar model. This has been made, and the result was not consistent, producing an *R*-factor of about 0.100, compared to the *R*-factor in the range 0.010−0.020 found for the mixed 2/3 tetracoordinated−1/3 pentacoordinated model, i.e. with 1/3 of the overall Pt sites pentacoordinated with the sulfur in the apical position on the Pt.

UV−Visible Absorption. Optical characterization of pristine samples has been reported in a previous work;[17] a sharp peak at wavelengths falling in the range 358−375 nm was observed for all the oligomers (number of repeat units 4−10 up to 50) due to $\pi-\pi^*$ transitions of the organic moiety and associated to the first singlet excited-state extending throughout the macromolecule. As a consequence of the reaction with H_2S, a peak at 357 nm is expected to appear as suggested by the literature;[7] unfortunately, the absorption spectra of Pt poly ynes are quite broad, and their maximum absorption wavelengths values are too close to 357 nm to distinguish a proper shoulder. Nevertheless, a fwhm increase was observed in UV−visible spectra for H_2S-containing samples with respect to the fwhm values estimated for H_2S-free samples spectra, as evidenced by UV−visible data that are summarized in Table 4 and by the superimposition of absorption spectra reported in Figure 8.

The spectra of pristine samples displayed $\pi-\pi^*$ absorption bands red-shifted with respect to the organic monomeric precursor DEBP (found at 290 nm), and the red shift increased by increasing the number of repetitive units in linear oligomers, i.e. going from sample **1** to samples **2** and **4**. This effect, that has been observed for analogous organometallic systems,[17,37] is indicative of an electronic delocalization occurring through the Pt centers, involving a contact between the π orbitals of the organic conjugated spacer with the Pt 5d and 6p orbitals.[39,40] Sample **3**, in which the organic moieties are disposed in cis configuration around the Pt centers, showed a λ_{max} value considerably lower than the tetranuclear all-trans oligomer **2**.

UV−visible spectra collected on samples **1**, **2**, and **4** are strictly similar to each other, as expected for systems of analogous chemical structure. As a consequence of the interaction with H_2S, the fwhm values of these spectra undergo a similar increase. This effect is much more evident for sample **3**, due to the lower λ_{max} value that allows the expected contribution at 375 nm due to H_2S to be observed. For the other samples, the H_2S contribution is almost completely superimposed on the main absorption band and is not distinguishable in the spectrum.

As a final observation, despite the severe experimental conditions used here for the gas exposure, some attempts have been made to test the reversibility of the Pt−S linkage after EXAFS measurements, for instance, by N_2 gas fluxing or by dissolving H_2S by means of chloroform and dichloromethane. Neither of these procedures succeeded, probably because of the high stability of the pentacoordinated complex, which was obtained under such severe experimental conditions. Actually, the first objective of our work at this stage was to verify that the main reason for the already assessed interaction between Pt-poly ynes and sulfur-containing gases is the transition metal, and that, conversely, the aromatic moieties of the organometallic macromolecules do not play a key role in the process. In the future, we plan to test our systems with smaller and controlled amounts of gas at lower pressure, in order to check the saturation conditions and test the reversibility of the interaction.

The adduct structure suggested by EXAFS data analysis results in excellent agreement with the structure suggested by the literature for the SO_2 adducts of similar Pt compounds. The UV−visible absorption spectra have also been collected, and a broadening of the absorption band around 360 nm confirms the presence of sulfur-containing compounds.[7]

Conclusions

The interaction of Pt-containing organometallic poly ynes with H_2S molecules has been investigated for one complex and three oligomers differentiated in both chain length (4, 9 repetitive units) and conformation (cis or trans). Several techniques, i.e. XPS, EXAFS, and UV−visible absorption spectroscopies, have been employed on purpose to carry on an extensive characterization of the four samples before and after exposure to H_2S. In this first approach to the study of these samples we have considered reaction conditions that facilitated the bonding of H_2S to the Pt systems. Our plan considers further investigations under more controlled exposure conditions. As a result of our study, the chemical interaction arising between Pt(II) centers and sulfur atoms has been assessed as evidenced by XPS Pt4f and S2p spectral analysis. Furthermore, the S/Pt atomic ratio of 1/3 for all samples, as estimated by XPS, suggests that in the experimental conditions considered here (Pt−poly yne samples exposed to H_2S gas at 500 mbar) the adsorption undergoes saturation. XAS data analysis suggested a square-pyramidal geometry around the transition metal with H_2S in the apical position for the pentacoordinated platinum units.

Acknowledgment. We gratefully acknowledge all the GILDA beamline staff for the support during measurements. We also thank Prof. A. Martorana and Dr. F. Giannici of the University of Palermo and Dr. A. Longo of the ISMN of the CNR for lending us the chemical cell.

References and Notes

(1) Speight, J. G. *The Chemistry and Technology of Petroleum*, 2nd ed.; Dekker: New York, 1991.

(2) Stern, A. C.; Boubel, R. W.; Turner, D. B.; Fox, D. L. *Fundamentals of Air Pollution*, 2nd, ed.;Academic Press: Orlando, FL, 1984.

(3) Thomas, J. M.; Thomas, W. J. *Principles and Practice of Heterogeneous Catalysis*; VCH: New York, 1997; Chapt. 6.

(4) Rodriguez, J. A.; Jirsak, T.; Pérez, M.; Chaturvedi, S.; Kuhn, M.; Gonzalez, L.; Maiti, A. *J. Am. Chem. Soc.* **2000**, *122*, 12362.

(5) Rodriguez, J. A.; Jirsak, T.; Pérez, M.; Chaturvedi, S. *J. Chem. Phys.* **1999**, *111* (17), 8077.

(6) Wang, Y.; Whang, S.; Zhao, Y.; Zhu, B.; Kong, F.; Wang, D.; Wu, S.; Huang, W.; Zhang, S. *Sens. Actuators B* **2007**, *125*, 79.

(7) Albrecht, M.; Gossage, R. A.; Lutz, M.; Spek, A. L.; van Koten, G. *Chem. Eur. J.* **2000**, *6* (8), 1431.

(8) Long, N. J.; Williams, C. K. *Angew. Chem.* **2003**, *115*, 26902722;. *Angew. Chem. Int. Ed.* **2003**, *42*, 2586 and references therein.

(9) Jones, S. C.; Coropceanu, V.; Barlow, S.; Kinnibrugh, T.; Timofeeva, T.; Brédas, J.-L.; Marder, S. R. *J. Am. Chem. Soc.* **2004**, *126*, 11782.

(10) Shull, T. H.; Kushmerick, J. G.; Patterson, C. H.; George, C.; Moore, M. H.; Pollack, S. K.; Shashidahr, R. *J. Am. Chem. Soc.* **2003**, *125*, 3202.

(11) Battocchio, C.; Fratoddi, I.; Russo, M. V.; Polzonetti, G. *Chem. Phys. Lett.* **2004**, *400*, 290.

(12) Polzonetti, G.; Carravetta, V.; Ferri, A.; Altamura, P.; Alagia, M.; Richter, R.; Russo, M. V. *Chem. Phys. Letters* **2001**, *340*, 449.

(13) Battocchio, C.; Fratoddi, I.; Iucci, G.; Russo, M. V.; Goldoni, A.; Parent, P.; Polzonetti, G. *Mater. Sci. Eng., C* **2007**, *27*, 1338.

(14) Caliendo, C.; Verona, E.; D'Amico, A.; Furlani, A.; Infante, G.; Russo, M. V. *Sens. Actuators B* **1995**, *24*−*25*, 670.

(15) Penza, M.; Cassano, G.; Sergi, A.; Lo Sterzo, C.; Russo, M. V. *Sens. Actuators B* **2001**, *81*, 88.

(16) Caliendo, C.; Fratoddi, I.; Russo, M. V. *Appl. Phys. Lett.* **2002**, *80* (25), 4849.

(17) Fratoddi, I.; Battocchio, C.; La Groia, A.; Russo, M. V. *J. Polym. Sci. A: Polym. Chem.* **2007**, *45*, 3311.

(18) Battocchio, C.; D'Acapito, F.; Fratoddi, I.; La Groia, A.; Polzonetti, G.; Roviello, G.; Russo, M. V. *Chem. Phys.* **2006**, *328* (1−3), 269.

(19) Swift, P.; Shuttleworth, D.; Seah, M. P. *Practical Surface Analysis by Auger and X-ray Photoelectron Spectroscopy*; Briggs, D., Seah, M. P., Eds.; J. Wiley & Sons: Chichester, 1983; Chapt. 5 and appendix 3.

(20) Shirley, D. A. *Phys. Rev. B.* **1972**, *5* (12), 4709.

(21) Lee, P.; Citrin, P.; Eisenberger, P.; Kincaid, B. *Rev. Mod. Phys.* **1981**, *53*, 769.

(22) Pascarelli, S.; Boscherini, F.; D'Acapito, F.; Hardy, J.; Meneghini, C.; Mobilio, S. *J. Synchrotron Radiat.* **1996**, *3*, 147.

(23) Longo, A.; Balerna, A.; D'Acapito, F.; D'Anca, F.; Giannici, F.; Liotta, L. F.; Pantaleo, G.; Martorana, A. *J. Synchrotron Radiat.* **2005**, *12*, 499.

(24) Newville, M.; Livins, P.; Yacoby, Y.; Stern, E. A.; Rehr, J. J. *Phys. Rev. B* **1993**, *47*, 14126.

(25) Ravel, B.; Newville, M. *J. Synchrotron Radiat.* **2005**, *12* (4), 537.

(26) Rehr, J. J.; Albers, R. C. *Rev. Mod. Phys.* **2000**, *72*, 621.

(27) Fratoddi, I.; Delfini, M.; Sciubba, F.; Hursthouse, M. B.; Ogilvie, H. R.; Russo, M. V. *J. Organomet. Chem.* **2006**, *691*, 5920.

(28) Grim, S. O.; Keiter, R. L.; McFarlane, W. *Inorg. Chem.* **1967**, *6* (6), 1133.

(29) Springborg, M. J. *Solid State Chem.* **2003**, *176*, 311.

(30) http://cars9.uchicago.edu/ifeffit/Documentation, accessed July 14, 2008.

(31) Folkesson, B.; Larsson, R. *J. Electron Spectrosc. Relat. Phenom.* **1982**, *26* (2), 157.

(32) Grim, S. O.; Matienzo, L. J.; Swartz, W. E., Jr *Inorg. Chem.* **1974**, *13* (2), 447.

(33) Atzei, D.; De Filippo, D.; Rossi, A.;.; Caminiti, R.; Sadun, C. *Inorg. Chim. Acta* **1996**, *248*, 203.

(34) Atzei, D.; De Filippo, D.; Rossi, A.; Porcelli, M. *Spectrochim. Acta A* **2001**, *57*, 1073.

(35) Contini, G.; Turchini, S.; Di Castro, V.; Polzonetti, G.; Marabini, A. M. *Appl. Surf. Sci.* **1992**, *59*, 1.

(36) Rodriguez, J. A.; Chaturvedi, S.; Jirsak, T.; Hrbek, J. *J. Chem. Phys.* **1998**, *109*, 4052, and references therein.

(37) Campbell, C. T.; Koel, B. E. *Surf. Sci.* **1987**, *183*, 100.

(38) Nilsson, D.; Watcharinyanon, S.; Eng, M.; Li, L.; Moons, E.; Johansson, L. S. O.; Zharnikov, M.; Shaporenko, A.; Albinsson, B.; Må, J. *Langmuir* **2007**, *23*, 6170.

(39) Dray, A. E.; Wittmann, H. F.; Friend, R. H.; Donald, A. M.; Khan, M. S.; Lewis, J.; Johnson, B. F. G. *Synth. Metal* **1991**, *871*, 41.

(40) Wittmann, H. F.; Fuhrmann, K.; Friend, R. H.; Khan, M. S.; Lewis, J. *Synth. Metal* **1996**, *56*, 55.

JP803119J